Short and long range 2D 15N-15N NMR correlations among peptide groups by novel solid state dipolar mixing schemes

Sungsool Wi (sungsool@magnet.fsu.edu)
Florida State University
Conggang Li
National Center for Magnetic Resonance in Wuhan, Chinese Academy of Sciences
Karen Pham
University of Colorado at Denver
Woonghee Lee
University of Colorado at Denver
Lucio Frydman
Weizmann Institute of Sciences

Research Article

Keywords: 15N-15N correlations, protein structure, dipolar-driven recoupling, chirped pulses

Posted Date: July 7th, 2023

DOI: https://doi.org/10.21203/rs.3.rs-3140402/v1

Additional Declarations: No competing interests reported.

Version of Record: A version of this preprint was published at Journal of Biomolecular NMR on December 16th, 2023. See the published version at https://doi.org/10.1007/s10858-023-00429-0.

Short and long range 2D ^{15}N-^{15}N NMR correlations among peptide groups by novel solid state dipolar mixing schemes

Sungsool Wi,[1*] Conggang Li,[2] Karen Pham,[3] Woonghee Lee,[3] and Lucio Frydman[1,4*]

[1] National High Magnetic Field Laboratory, Florida State University, Tallahassee, Florida 32304, USA

[2] Key Laboratory of Magnetic Resonance in Biological Systems, State Key Laboratory of Magnetic Resonance and Atomic and Molecular Physics, National Center for Magnetic Resonance in Wuhan, Wuhan Institute of Physics and Mathematics, Innovation Academy for Precision Measurement Science and Technology, Chinese Academy of Sciences, Wuhan, 430071, P.R. China

[3] Department of Chemistry, University of Colorado at Denver, Denver, CO 80217-3364, USA

[4] Department of Chemical and Biological Physics, Weizmann Institute of Sciences, Rehovot, Israel

* *Emails: sungsool@magnet.fsu.edu, lucio.frydman@weizmann.ac.il*

Abstract

A recently developed homonuclear dipolar recoupling scheme, Adiabatic Linearly FREquency Swept reCOupling (AL FRESCO), was applied to record two-dimensional (2D) ^{15}N-^{15}N correlations on uniformly ^{15}N-labeled GB1 powders. A major feature exploited in these ^{15}N-^{15}N correlations was AL FRESCO's remarkably low RF power demands, which enabled seconds-long mixing schemes when establishing direct correlations. These ^{15}N-^{15}N mixing schemes proved efficient regardless of the magic-angle spinning (MAS) rate and, being nearly free from dipolar truncation effects, they enabled the detection of long-range, weak dipolar couplings, even in the presence of strong short-range dipolar couplings. This led to a connectivity information that was significantly better than that obtained with spontaneously proton-driven, ^{15}N spin-diffusion experiments. An indirect approach producing long-range ^{15}N-^{15}N correlations was also tested, relying on short (ms-long) $^{1}H^{N}$-$^{1}H^{N}$ mixings schemes while applying AL FRESCO chirped pulses along the ^{15}N channel. These indirect mixing schemes produced numerous long-distance N_i-$N_{i\pm n}$ ($n = 2 - 5$) correlations, that might be useful for characterizing three-dimensional arrangements in proteins. Once again, these AL FRESCO mediated experiments proved more informative than variants based on spin-diffusion-based $^{1}H^{N}$-$^{1}H^{N}$ counterparts.

Keywords: ^{15}N-^{15}N correlations, protein structure, dipolar-driven recoupling, chirped pulses

Introduction

Homonuclear dipolar correlation schemes operating in unison with magic angle spinning (MAS), are widely used in solid-state NMR (SSNMR) spectroscopy for the structural characterization of selectively or uniformly labeled biological samples.[1-27] Most common among these schemes are methods that rely on first-order recoupling effects, such as RFDR[4] and DREAM;[7] although efficient and requiring short mixing times to achieve their correlations, such methods may suffer from dipolar truncation effects.[28] Thus, when applied to uniformly ^{13}C-labeled samples, these methods deliver mostly short-range ^{13}C-^{13}C dipolar correlations useful for peak assignment purposes, but not for establishing long-range structural constraints. Therefore, although slower in building up dipolar transfers, recoupling schemes based on second-order effects that are free from dipolar truncation,[15-17] have been utilized in examining weaker, long-range ^{13}C-^{13}C dipolar couplings. Such recoupling schemes include PDSD,[10-12] DARR,[15,16] RAD,[17] PARIS$_{xy}$,[20,21] SHANGHAI,[22] SHA+,[23,29,30] CORD,[25,26] MIRROR,[24] and AL FRESCO.[27] A common feature shared by these recoupling schemes is their utilization of ^{1}H-^{13}C heteronuclear dipolar interactions to broaden otherwise narrow ^{13}C-^{13}C rotational resonance conditions, and thereby facilitate ^{13}C-^{13}C spin-diffusion despite chemical shifts differences spanning a wide range of frequencies.[15,16] Second-order recoupling methods will usually require longer mixing times than first-order recoupling schemes, and each method will possesses its own strengths and weaknesses in terms of the "broadbandedness" of offset frequency differences over which it can recouple, of the MAS rates that it can tolerate, of the radiofrequency (rf) pulse strengths required, etc.[20-23,25-27,29] Still, in general, most second-order recoupling schemes have been successfully applied to ^{13}C-^{13}C dipolar correlation experiments in biomolecules.

Much fewer, by contrast, has been the execution of these experiments to the recoupling of ^{15}N-^{15}N spin pairs –characterized as they are by weaker dipolar interactions.[31-39] ^{15}N-^{15}N distance constraints, however, offer a unique potential in the characterization of secondary structures and their three-dimensional arrangements, particularly when dealing with uniformly ^{15}N-labeled proteins. 2D correlations targeting the amide region will then provide one nitrogen resonance per amino acid residue, thereby facilitating both the assignment and the structural constraint of peptides in the protein. Still, ^{15}N-^{15}N SSNMR dipolar correlations have usually been reported for $^{15}N_i$-$^{15}N_{i\pm1}$ connectivities between nearby residues.[32,35-39] Major limitations arising when seeking longer correlations in uniformly ^{15}N-labeled proteins include: 1) the aforementioned weakness of the ^{15}N-^{15}N dipolar interaction, which is only ≈1/6 as strong as a similarly-distanced ^{13}C-^{13}C dipolar interaction; 2) the relatively long ^{15}N-^{15}N distances involved when considering non-consecutive –and even consecutive– peptidic residues; and 3) the relatively narrow chemical shift dispersion of amide ^{15}Ns in proteins (~35 ppm), leading to an overlap between ^{15}N peaks that can be severe –particularly when the crystallinity of a protein sample is poor and when seeking multiple correlations. As a result of the first two features, second-order recoupling methods applied to ^{15}N-^{15}N correlations require significantly longer mixing times than their ^{13}C-^{13}C counterparts – lasting up to a few seconds. Thus, among all the 2nd-order homonuclear recoupling schemes mentioned above, only the proton-driven spin-diffusion (PDSD) scheme that does not require any rf pulses during the mixing, has been so far utilized to achieve these ^{15}N-^{15}N correlations. The relative inefficiency of PDSD, however, also means that the NMR signals will decay significantly by T_1 relaxation effects during the long mixing times involved in such experiments. Proton-assisted recoupling (PAR) methods relying on the third spin-assisted recoupling (TSAR) mechanism[18,19] have been employed to obtain faster ^{15}N-^{15}N signal transfers leading to the

establishment of longer $^{15}N_i$-$^{15}N_{i\pm n}$ ($n \geq 2$) constraints,[33] although some $^{15}N_i$-$^{15}N_{i\pm1}$ correlations available from the PDSD scheme were not visible by PAR when carried out on the same sample system.[32,33,40] This work explores the application of the recently proposed AL FRESCO scheme, to obtain this kind of ^{15}N-^{15}N correlations in proteins under a variety of conditions. Advantages of the ensuing approach are illustrated, and potential extensions of this method briefly discussed.

Results

This work explored the application of direct ^{15}N-^{15}N (Figure 1a), and indirect $^{1}H^{N}$-$^{1}H^{N}$-driven (Figure 2a) 2D AL FRESCO schemes (Figure 1b), to obtain 2D ^{15}N-^{15}N correlations under MAS. The AL FRESCO scheme[27] was originally applied to recouple ^{13}C-^{13}C dipolar interactions, and proved particularly efficient under fast MAS rates (~ 60 kHz). AL FRESCO involves storing the t_1-encoded X-nuclei polarization along the z-axis (X=^{13}C or ^{15}N), and employing a phase-modulated chirped pulse –such as the wideband, uniform rate, smooth truncation (WURST)[41] or the hyperbolic secant (HS) [42,43] pulse– on the ^{1}H channel, in order to achieve the recoupling between the non-equivalent low-γ nuclei. This chirped mixing rf pulse can be relatively weak, with an amplitude ν_{rf}= 5 ~ 20 kHz regardless of the MAS rate employed –low-powers becoming a significant advantage when assessing long X-X distances, characterized by MAS-averaged couplings demanding extended mixing times. The chirped mixing pulses will then reintroduce the ^{1}H-X heteronuclear dipolar coupling despite the MAS averaging, by repeatedly satisfying the rotary resonance condition:

$$\nu_{eff}(^1H) = \left[\left\{\Omega_H + \frac{\mathrm{BW}}{2} - \left(\frac{\mathrm{BW}}{t_p}\right)t\right\}^2 + \left\{\nu_{rf}^{env}(t)\right\}^2\right]^{1/2} = \nu_r, \quad (1)$$

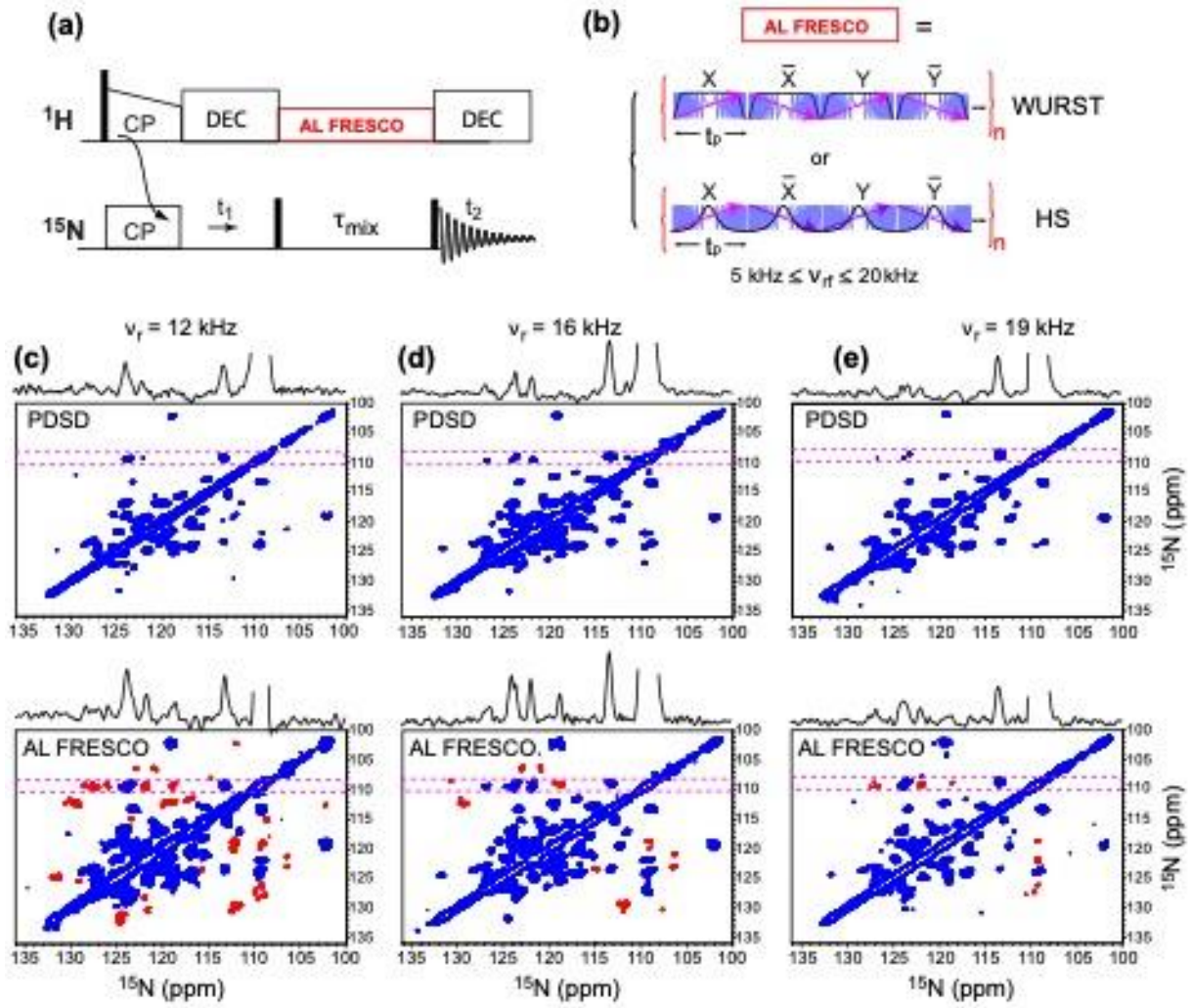

Figure 1. The ^{15}N-^{15}N PDSD and AL FRESCO correlation spectra acquired on a doubly-labeled GB1 sample. (a,b) Chirped pulse AL FRESCO sequence implemented within the framework of 2D homonuclear dipolar correlation spectroscopy. A single chirp pulse or a series of phase-alternating chirp pulses with a relatively weak rf pulse (5 kHz $\leq \nu_{rf} \leq$ 20 kHz) were employed; ^{15}N-^{15}N PDSD correlation spectra would do nothing on the ^{1}H channel over the mixing period. (c-e) 2D data acquired by spin diffusion (top row) and AL FRESCO schemes (bottom row) at MAS rates of ν_r = 12 kHz (c), 16 kHz (d), and 19 kHz (e). Extra ^{15}N-^{15}N correlation peaks found in the AL FRESCO scheme but not in PDSD, are indicated by red contours. A horizontal projection taken in the 108~110 ppm range is shown on top of each 2D spectrum. The number of t_1 increments (n_{t1}), total number of scans (ns), dwell time of the indirect time domain (dw_{t1}), and acquisition delay (d_1) used for each spectrum were n_{t1} = 160, ns = 48, dw_{t1} = 250 μs, and d_1 = 1.2 s, respectively. Double ^{13}C/^{15}N labeling was used for facilitating the peaks' assignments (see Supporting Information). Although ^{13}C decoupling was assayed, it did not afford any improvements in the observed lineshapes along either dimension and hence its use was discontinued.

where $\nu_{eff}(^1H)$ is the effective ^{1}H rf strength, Ω_H is the ^{1}H frequency offset, BW is the chirp's sweep bandwidth, t_p is the chirp's pulse length, $\nu_{rf}^{env}(t)$ is the time-varying rf pulse strength

considered with the envelope shape of the chirp, and ν_r is the sample MAS rate. The ^{1}H-X heteronuclear dipolar couplings thus introduced can then reestablish a homonuclear X_1-X_2 coupling, by broadening the homonuclear transfer otherwise given by a narrow rotational resonance condition, $\Delta\Omega = \nu_{X_1} - \nu_{X_2} = \nu_r$. As described previously,[27] AL FRESCO mixing effectiveness also benefits from the application of an undersampled chirped scheme whereby $1/\Delta t \ll BW$, where Δt is the dwell time used to clock out the pulse. This deviates from the usual Nyquist sampling condition $1/\Delta t \geq BW$ required to avoid frequency folding, and implies that frequency points within the $1/\Delta t$ frequency window are addressed multiple times during the course of a single frequency sweep –in other words, that the X_1-X_2 signal transfer conditions within a $1/\Delta t$ window are satisfied multiple times. This ends up enhancing the transfer efficiency for a given mixing time

Figures 1c-1e compare variable-rate 2D MAS ^{15}N-^{15}N correlation spectra collected on uniformly ^{15}N,^{13}C-labeled GB1, using a PDSD mixing scheme (first row) with τ_{mix} = 6.25 s, and the AL FRESCO mixing scheme (second row) with a mixing time of 6.25 s and an average effective rf pulse strength of $\overline{\nu_{rf}^{env}}$ = 5.3 kHz. The MAS spinning rates used were 12 kHz (c), 16 kHz (1d), and 19 kHz (1e), respectively. In each case, four identical HS mixing pulses (1% truncation) were used in series, while shifting phases and changing the direction of the sweep as shown in the figure, with t_p = 1.25 s, $\Delta t = 3/\nu_r$, $N = t_p/\Delta t$, and BW= 80 kHz. Thus, the overall AL FRESCO mixing time was $4N\Delta t$ = 6.25 s in all cases. As the MAS rate increases the number of ^{15}N-^{15}N cross-peaks in both PDSD and AL FRESCO spectra decrease; however, at each MAS rate, the AL FRESCO experiment clearly delivers ^{15}N-^{15}N cross-peaks (red contours) that are missing in the conventional PDSD spectrum. This observation can be justified by the fact that AL FRESCO, as a derivative of the dipole-assisted rotational resonance (DARR) technique, will produce X_1-X_2 cross-peaks more efficiently than a non-recoupled PDSD experiment. The

Supporting Information presents simulations that further support this premise (see Supporting Figures S1a, S1b). Notice as well that DARR would require its rf pulse power to increase with MAS rate in order to keep on matching a $\nu_{rf} = \nu_r$ condition, whereas AL FRESCO requires much weaker rf powers even as the MAS rate increases, owing to its reliance on effective fields. The data in Figure 1 are complemented with PDSD and AL FRESCO GB1 spectra measured at shorter mixing times (2 s) at three different MAS rates, ν_r = 12, 16, and 19 kHz. As can be appreciated from Supporting Figure S2, these spectra exhibit significantly fewer cross peaks than these spectra measured with τ_{mix} = 6.25 s; yet also in that instance, AL FRESCO reveals connectivities that are lost in the PDSD data.

An alternative route that can significantly increase the number of ^{15}N-^{15}N correlations while reducing the length required by the mixing time, is to employ a $^{1}H^{N}$-$^{1}H^{N}$ mixing method. This calls for an ^{15}N →H→H→^{15}N pulse scheme of the kind shown in Figure 2a[44-47] where, after the first ^{1}H-^{15}N CP step, ^{15}N magnetizations that evolved over a time t_1 are sent back to the ^{1}H reservoir via a 2nd ^{15}N→^{1}H CP step for longitudinal $^{1}H^{N}$-$^{1}H^{N}$ mixing. This can proceed either by spontaneous spin diffusion (SD) or aided by AL FRESCO mixing pulses, applied this time on the ^{15}N species. Following this, ^{1}H magnetizations are transferred again to the ^{15}N channel for detection via a final ^{1}H→^{15}N CP step; chirped ^{15}N pulses would then be used in this AL FRESCO scheme to aid the $^{1}H^{N}$-$^{1}H^{N}$ mixing.

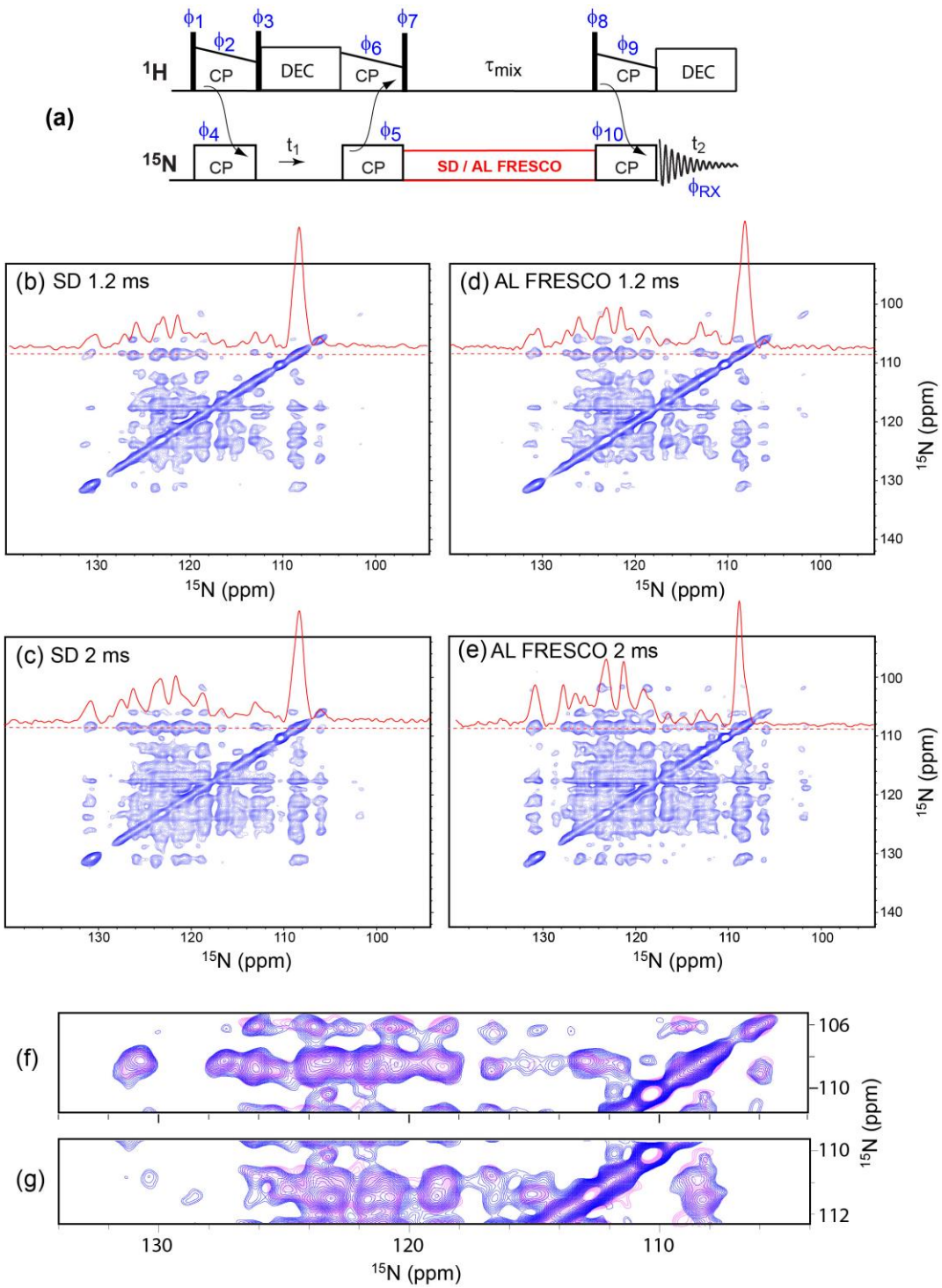

Figure 2. (a) ^{15}N-^{15}N 2D correlation sequence implemented using a $^1H^N$-$^1H^N$ mixing scheme aided by either spontaneous spin diffusion (SD) or AL FRESCO pulses applied on the ^{15}N channel. Black lines indicate 90˚ pulses. Pulse phases: $\phi_1 = (x)_2, (-x)_2, (y)_2, (-y)_2, (-x)_2, (x)_2, (-y)_2, (y)_2$; $\phi_2 = (-y)_4, (x)_4, (y)_4, (-x)_4$; $\phi_3 = (-x)_2, (x)_2, (-y)_2, (y)_2, (x)_2, (-x)_2, (y)_2, (-y)_2$; $\phi_4 = y$; $\phi_5 = y$; $\phi_6 = -y, y$; $\phi_7 = x$; $\phi_8 = -x$; $\phi_9 = y$; $\phi_{10} = (y)_2, (-y)_2, (-x)_2, (x)_2, (-y)_2, (y)_2, (x)_2, (-x)_2$; ϕ_{rx}= -y, y, -y, y, x, -x, x, -x, y, -y, y, -y, -x, x, -x, x. (b-e) ^{15}N-^{15}N correlation spectra of ^{15}N-labeled GB1 measured using $^1H^N$-$^1H^N$ SD and $^1H^N$-$^1H^N$ AL FRESCO sequences with mixing times of 1.2 ms (b,d) and 2 ms (c,e). While employing the MAS spinning rate ν_r = 16 kHz, the number of

t_1 increments (n_{t1}), total number of scans (ns), dwell time used in the indirect time domain (dw_{t1}) and acquisition delay time (d_1) used in each experiment were n_{t1} = 150, ns = 160, dw_{t1} = 250 μs and d_1= 2 s, respectively. Comparing the SD (pink) and AL FRESCO (blue) derived strips collected for the 2 ms mixing case are shown separately in (f) and (g).

Figures 2b-2e show ^{15}N-^{15}N correlation spectra of GB1 collected in this fashion, by relying on spontaneous $^{1}H^{N}$-$^{1}H^{N}$ spin diffusion (2b, 2c) and on AL FRESCO (2c, 2e) mixing schemes. These MAS data were collected at ν_r = 16 kHz, using mixing times of τ_{mix} = 1.2 ms (2b, 2d) and 2 ms (2c, 2e); further details of the experimental parameters are specified in the figure caption and in the Experimental. Standing out against the low-γ-based dipolar mixing experiments in Figure 1, are the many additional ^{15}N-^{15}N correlations visible in these indirect $^{1}H^{N}$-$^{1}H^{N}$ mixing experiments –despite their very short mixing times. Furthermore, as can be seen by comparing the spectra measured by $^{1}H^{N}$-$^{1}H^{N}$ SD (2b and 2c) and $^{1}H^{N}$-$^{1}H^{N}$ AL FRESCO (2d and 2e), additional ^{15}N-^{15}N correlations are once again visible for the latter for both 1.2 ms and 2 ms mixing times (e.g., compare the 1D projection spectrum taken at ~109 ppm and shown in each 2D spectrum). This is more clearly illustrated by the strips extracted at ≈108 and 111 ppm for the two experiments measured with 2 ms, which show additional ^{15}N-^{15}N correlations from the AL FRESCO scheme (Figures 2f, 2g). A more thorough cross-comparison among all these experiments is presented in Supporting Tables S2 and S3, which summarize the $^{15}N_i$-$^{15}N_j$ cross-peak correlations obtained both by the direct ^{15}N-^{15}N and indirect $^{1}H^{N}$-$^{1}H^{N}$ correlation experiments presented in Figures 1 and 2. The first of these Tables summarizes correlations between nearest neighboring amino acids in the peptide sequence, whereas the second focuses on distant correlations. Table 1 complements these data by summarizing the number of N_i -N_j correlations found by 2D ^{15}N-^{15}N correlation experiments carried out so far on U-^{15}N-GB1, including conventional PDSD,[32] PAR,[33] and the ^{15}N-^{15}N AL FRESCO and $^{1}H^{N}$-$^{1}H^{N}$ SD and AL FRESCO schemes. The $^{1}H^{N}$-$^{1}H^{N}$ AL FRESCO

scheme appears to give more correlations than any other alternative –including those that have been reported in the U-^{15}N-GB1 solid-state NMR literature so far.[32,33]

Table 1. Number of $N_i - N_j$ ($j = i \pm n$) correlations found in GB1 by various mixing schemes.

n	Experiment	α-helix	β-sheet	loop	loop ↔ β-sheet	α-helix ↔ loop	loop ↔ loop	β–sheet ↔ β–sheet
1	^{15}N-^{15}N PDSD[1]	10	6	10	10	3		
	^{15}N-^{15}N PAR[2]	12	1	8	5	2		
	^{15}N-^{15}N AL FRESCO	10	8	9	6	3		
	^{1}H^{N}-^{1}H^{N} SD	13	3	5	7	3		
	^{1}H^{N}-^{1}H^{N} AL FRESCO	14	10	12	14	4		
≥2	^{15}N-^{15}N PDSD[1]	7		1	1	1		
	^{15}N-^{15}N PAR[2]	3			1		1	3
	^{15}N-^{15}N AL FRESCO	16	2	2	1	1	3	4
	^{1}H^{N}-^{1}H^{N} SD	27	1	2	3	4	6	4
	^{1}H^{N}-^{1}H^{N} AL FRESCO	30	3	5	8	5	10	22

[1] Reference 32; [2] Reference 33.

For completion, Figures 3a and 3b compare the N_i-N_j correlations obtained by the direct ^{15}N-^{15}N AL FRESCO and by the indirect ^{1}H^{N}-^{1}H^{N} AL FRESCO scheme, respectively. Additionally shown in Figure 3c are partial overlays from the 108-112, 115-119 and 131-134 ppm regions (F_1 domain), clearly evidencing the additional N_i-N_j correlations visible upon using the ^{1}H^{N}-^{1}H^{N} mixing.

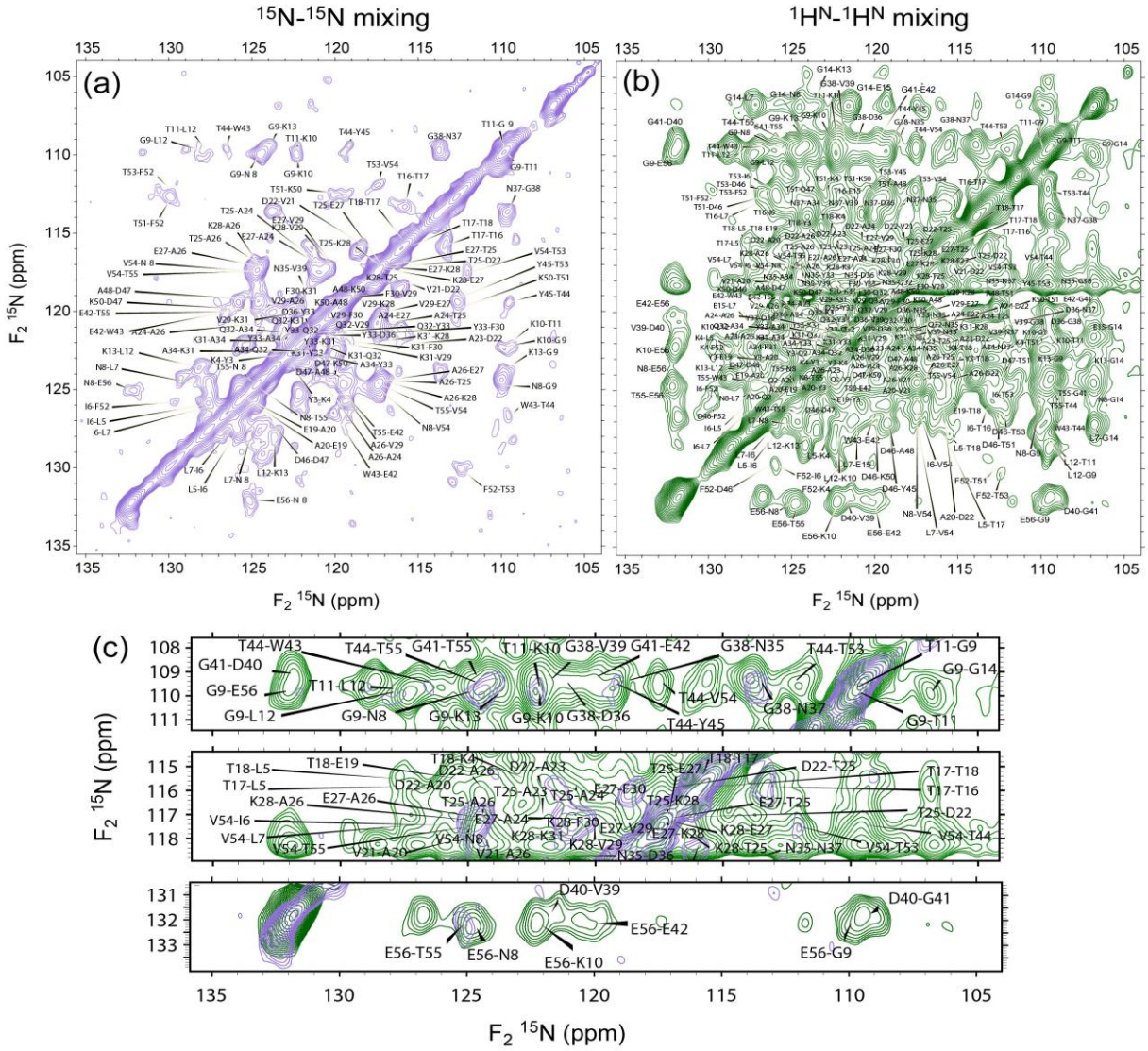

Figure 3. Peak assignments and comparisons between the ^{15}N-^{15}N correlation spectra obtained (a) by the direct ^{15}N-^{15}N AL FRESCO, and (b) by the indirect ^{1}H^{N}-^{1}H^{N} AL FRESCO scheme. The spectrum shown in Fig. 3a is identical to that shown in the second row of Fig. 1c and the spectrum shown in Fig. 3b is the same as that shown in Fig. 2c. (c) Partial spectra extracted from panels (a) and (b) to enlarge various F1 regions, and further clarify the observed N_i-N_j correlations.

Discussion

^{15}N-based AL FRESCO mixing experiments do not appear substantially better than PDSD-based ones when targeting nearest neighbor connectivities, but exceed the latter performance when seeking longer distances. Indeed most ^{15}N-^{15}N correlations observed in the PDSD experiment,[32]

are of the N_i-$N_{i\pm1}$ type: 10 are in GB1's α-helix, 6 in its β-sheet, 10 in the loop region, and 13 at the loop ↔ β-sheet and loop ↔ α-helix interfaces. In addition, a few N_i-$N_{i\pm2}$ correlations are also observed: 7 in the α-helix, 1 in a loop, and 2 from the interface loop ↔ α-helix and loop ↔ β-sheet. Being less affected by dipolar truncation, PAR shows a better ability to detect longer N_i-$N_{i\pm n}$($n\geq2$) correlations:[33] data revealed one such loop ↔ loop correlation; and 3 β-sheet↔β-sheet ones –even if some N_i - $N_{i\pm1}$ and N_i - $N_{i\pm2}$ correlations visible in the PDSD experiment, are remarkably missing from the PAR experiment (see Table 1 and Supporting Tables S2 and S3). The ^{15}N-^{15}N AL FRESCO experiment shows an increase in the number of N_i - $N_{i\pm n}$ ($n \geq 2$) correlations over the former two experiments. The data show 3 such loop ↔ loop correlations, 4 β-sheet↔β-sheet correlations, 1 loop↔β-sheet correlation, and 1 α-helix↔loop (Table 1). The method also increases the number of N_i-$N_{i\pm2}$ correlations in the α-helix structure compared to the PDSD and PAR (Table 1 and Supporting Table S3).

$^1H^N$-$^1H^N$ schemes increase considerably both N_i-$N_{i\pm1}$ and N_i-$N_{i\pm n}$($n\geq2$) correlations, with the AL FRESCO version providing more correlations for every type of ^{15}N-^{15}N connectivity than SD. As can be seen from Supporting Table S3, the τ_{mix} = 2 ms AL FRESCO scheme provides multiple structurally-rich N_i - $N_{i\pm n}$ ($n \geq 2$) correlations, including contacts between different secondary structures (10 loop ↔ loop correlations, 22 β-sheet↔β-sheet correlations, 8 loop↔β-sheet correlations and 5 α-helix↔ loop correlations), as well as within the secondary structures (30 within the α-helix, 3 in the β-sheets, and 5 in the loop regions). Overall, 80 N_i-$N_{i\pm n}$($n\geq2$) correlations are detected by the indirect $^1H^N$-$^1H^N$ AL FRESCO scheme, whereas the direct ^{15}N-^{15}N AL FRESCO scheme only yields 28. Numerous of these N_i-$N_{i\pm n}$ (n = 3,4) correlations are found within the α-helix or between β and loop structures, whereas within the β-sheet only N_i-$N_{i\pm n}$

correlation with $n = 2$ are observed. This is because distances for the H_i^N-$H_{i\pm n}^N$ (n =3-4) correlations in the α-helix and β-loop motifs are in the 3.5~4.6 Å range, whereas the H_i^N-$H_{i\pm 2}^N$ distances in a β-sheet structure motif are 6.8~7.1 Å long. Still, if multiple β-sheet chains form parallel or antiparallel registries, inter-registry N_i-$N_{i\mp n}$ ($n \geq 2$) correlations between nearby β-sheet structures can still be detected by the $^1H^N$-$^1H^N$ AL FRESCO scheme, as can be seen from Table 1 and Supporting Table S3.

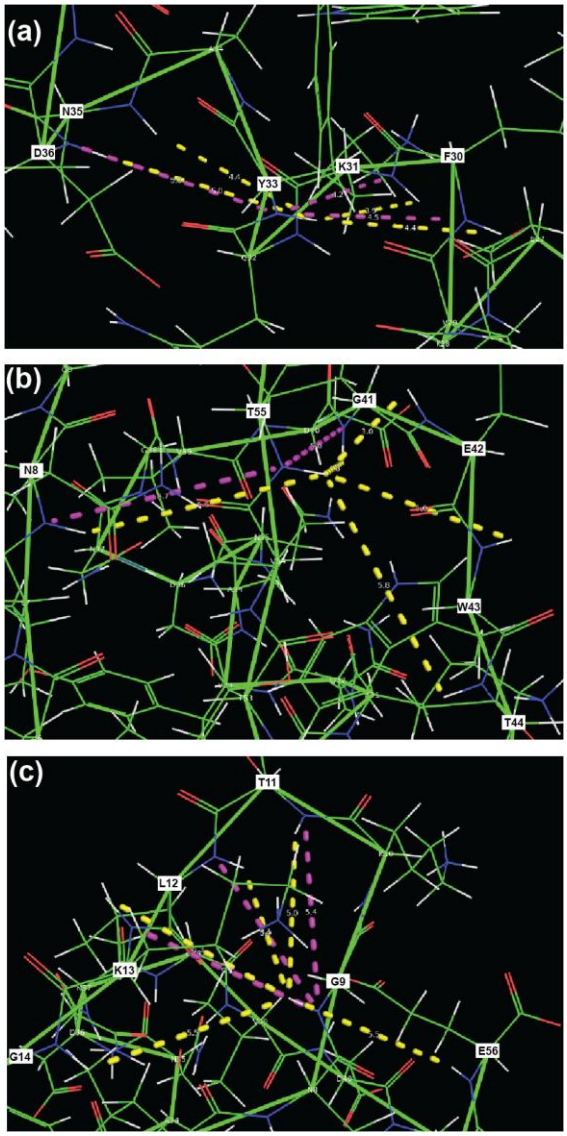

Figure 4. Examples of structural constraints, N_i-$N_{i\pm n}$ and H_i^N - $H_{i\pm n}^N$ (n>2), identified from the assigned correlations of the spectra shown in Figure 3 in typical α-helix, antiparallel β-sheet registry, and β-turn motifs. Dashed pink lines represent correlations revealed by the N_i-$N_{i\pm n}$ mixing experiments, and dashed yellow lines represent correlations revealed by the H_i^N-$H_{i\pm n}^N$ tests. Further details about these correlations are summarized in Table 2.

Figure 4 shows pictorial examples of long-range N_i-$N_{i\pm n}$($n \geq 2$) correlations found in α-helix (4a), β-sheet registry (4b), and β-loop (4c) motifs of GB_1, in the correlation data obtained by ^{15}N-^{15}N (6.5 s mixing time) and the $^1H^N$-$^1H^N$ (2 ms mixing time) AL FRESCO mixing schemes. Details of peak positions, distance constraints, and inter-residue distances n involved in these correlations are summarized in Table 2. In an α-helix structure (Figure 4a), the Y33-K31, Y33-F30 and Y33-D36 correlations are visible in the ^{15}N-^{15}N AL FRESCO scheme (pink dashed lines); an additional Y33-N35 correlation is visible when using

the indirect $^{1}H^{N}$-$^{1}H^{N}$ AL FRESCO mixing scheme (yellow dashed line). Figure 4b illustrates correlations formed between β-sheets and β-sheet structures in an antiparallel β-sheet registry for T55: the T55-G41 and T55-N8 correlations are visible from the direct ^{15}N-^{15}N AL FRESCO scheme, while additional T55-E42, T55-W43, and T55-T44 correlations appear when utilizing the indirect $^{1}H^{N}$-$^{1}H^{N}$ AL FRESCO scheme. Finally, Figure 4c illustrates the N_i - $N_{i\pm n}$ ($n \geq 2$) correlations for residue G9 with nearby residues in a β-loop motif. There, G9-T11, G9-L12, and G9-K13 correlations are visible with the direct ^{15}N-^{15}N AL FRESCO scheme, while G9-T11, G9-L12, G9-K13, G9-G14 and G9-E56 correlations also arise with the indirect $^{1}H^{N}$-$^{1}H^{N}$ AL FRESCO scheme. Other long-range N_i-$N_{i\pm n}$ ($n \geq 2$) correlations formed for each GB1 residue as examined by various mixing schemes, are summarized in the Table S3 of the Supporting Information.

Table 2. Representative N_i-N_j (n = j-i ≥2) correlations found in ^{15}N-^{15}N AL FRESCO and $^{1}H^{N}$-$^{1}H^{N}$ Al FRESCO mixing schemes.

Pair	N_i ppm	N_j ppm	n	N_i-N_j Distance (Å)	^{15}N-^{15}N 6.25 s	H_i^N-H_j^N Distance (Å)	$^{1}H^{N}$-$^{1}H^{N}$ 2 ms
T55 – N8	124.6	124.9	47	5.7	ϒ	5.9	ϒ
T55 - G41	124.6	109.2	14	4.9		4.5	ϒ
T55 - E42	124.6	120.0	13	3.9	ϒ	3.1	ϒ
T55 - W43	124.6	126.4	12	5.1		5.0	ϒ
T55 - T44	124.6	109.4	11	6.7		5.7	ϒ
Y33-D36	121.5	121.2	3	5.0	ϒ	5.0	ϒ
Y33-N35	121.5	118.7	2	4.4		4.4	ϒ
Y33 – F30	121.5	119.2	3	4.5	ϒ	4.4	ϒ
Y33 – K31	121.5	121.9	2	4.2	ϒ	3.8	ϒ
G9 – E56	109.8	132.0	47	5.5		5.4	ϒ
G9 – G14	109.9	106.8	5	6.9		5.7	ϒ
G9 – K13	109.8	123.7	4	5.3	ϒ	5.5	ϒ
G9 – L12	109.8	127.8	3	5.0	ϒ	3.7	ϒ
G9 – T11	109.8	109.7	2	5.4	ϒ	5.1	ϒ

***** Mutual correlations N_i-N_j and N_j-N_i are counted once as N_i-N_j.

Conclusion

This study examined the AL FRESCO mixing scheme as applied on uniformly ^{15}N,^{13}C-labeled GB1 to obtain ^{15}N-^{15}N correlations under a moderately spinning rates via direct ^{15}N-^{15}N and indirect $^{1}H^{N}$-$^{1}H^{N}$ mixing schemes. A significant number of correlations, particularly long-range N_i-$N_{i\pm n}$($n\geq2$), were produced with both cases. The usefulness of ^{15}N-^{15}N correlations relying on AL FRESCO schemes, particularly via $^{1}H^{N}$-$^{1}H^{N}$ mixing, is therefore proven for examining the protein secondary structures and three-dimensional arrangements in the solid-state NMR of polycrystalline systems. Overall, the constraints arising from the $^{1}H^{N}$-$^{1}H^{N}$ AL FRESCO scheme should help determine the three-dimensional arrangement of secondary structures in protein structures. We are currently extending the $^{1}H^{N}$-$^{1}H^{N}$ AL FRESCO scheme further to the case of ^{1}H-detection mode under a very fast MAS rate, as well as to experiments that –by introducing an additional ^{13}C-based dimension, can perform similar kind of correlations with the spectral enhancement afforded by 3D NMR.

Experimental Details

Sample. [U-^{13}C,^{15}N] GB1 was expressed in E. Coli BL21-(DE3) cells that grew in minimal media (1 g/L $^{15}NH_4Cl$, 2 g/L ^{13}C glucose). This double-labeling was chosen over the simpler ^{15}N-only labeling for facilitating the peaks' assignments. Protein expression was induced with 1 mM isopropyl-β-D-thiogalactoside for 4 hours. The protein was purified by anion exchange using a Q-Sepharose FF column, followed by gel filtration on a Superdex75 column. Peak fractions were pooled and concentrated with Centriplus 3 kDa MWCO filters, and the buffer solution was thoroughly exchanged to 20 mM sodium phosphate at pH 8.0. To obtain highly resolved ^{15}N NMR spectra a microcrystalline GB1 powder was prepared by following the precipitation procedure of Franks et al.[40] In this, about 3.6 mL aliquots of a mixture of isopropanol (1.2 mL) and 2-

methylpentane-2,4-diol (2.4 mL) were added dropwise to 1.2 mL of a 30 mg/mL solution of GB1 in phosphate buffer (pH 5.5), while mixing the solution thoroughly using a vortex. The resultant solution was left at room temperature for about 30 minutes and then, the milky protein precipitate was centrifugated. The pellet was packed into 3.2 mm pencil type NMR rotors by centrifugation using a home-made swing bucket for rotor packing.

NMR experiments. NMR experiments were carried out on an 18.8 T magnet equipped with a Bruker Avance III HD console using a 3.2 mm ^{1}H-X-Y low-E NHMFL-built MAS probe. MAS spinning rates of 12, 16 and 19 kHz were used for the direct ^{15}N-^{15}N correlations scheme, and 16 kHz for the indirect scheme relying on the $^{1}H^{N}$-$^{1}H^{N}$ mixing. The sample temperature was regulated at -10°C (measured at the sample compartment) by flowing a nitrogen gas stream generated from a liquid nitrogen tank via an FTS cooling system. ^{1}H, ^{13}C and ^{15}N 90° pulses were adjusted to 2.5 μs, 5 μs, and 9 μs, respectively, for all the experiments. For the direct ^{15}N-^{15}N mixing scheme, an optimal ^{1}H-^{15}N cross-polarization (CP) condition at each spinning rate was found at ν_1 (^{15}N) = 27 kHz and ν_1(^{1}H) = 50 ~ 70 kHz depending on the MAS rate; a rectangular pulse along the ^{15}N channel and a simultaneous ramped (70%–110%) spin-lock pulse along ^{1}H channel for 700 μs, were used for CP. For the indirect $^{1}H^{N}$-$^{1}H^{N}$ mixing scheme,[44,45] 700 μs long rectangular spin-lock pulses with an identical ^{15}N pulse power, ν_1(^{15}N) = 27 kHz, were used along the ^{15}N channel at the 1st ^{1}H-^{15}N CP; the 2nd ^{15}N-^{1}H CP lasted 240 μs, and the 3rd ^{1}H-^{15}N CP for 420 μs. A ramped (70%–110%) spin-lock pulse was applied simultaneously along the ^{1}H channel in each case with rf powers of ν_1(^{1}H) = 54 kHz, 47 kHz, and 53 kHz, respectively. SPINAL-64[48] (90 kHz rf field) was applied for ^{1}H decoupling during the direct and indirect evolution/acquisition periods; no ^{13}C decoupling was used, as tests did not reveal any ^{15}N line shape improvements deriving from it.

Two-dimensional (2D) NCO/NCA MAS experiments (ν_r = 16 kHz)[49,50] were carried out for peak assignment purposes. The rf pulse parameters used were: first ^{1}H-^{15}N CP with $\nu_1(^{15}N)$ = 27 kHz and $\nu_1(^1H)$ = 68 kHz for 700 μs while applying a ramped spin-lock (70%-110%); second ^{15}N-^{13}C CP with $\nu_1(^{15}N)$ = 30 kHz and $\nu_1(^{13}C)$ = 45 kHz for 5 ms with a ramped spin-lock pulse (70%-110%) applied along ^{13}C while placing the ^{13}C's offset carrier frequency at CO peaks and Cα peaks for NCO and NCA, respectively. 128 t_1 slices were taken with a dwell time of 250 μs for both NCO and NCA. Each t_1 point was produced by coadding 128 scans with an acquisition delay time of 2 s.

Chirp mixing pulse design. Wideband, uniform rate, smooth truncation (WURST) and hyperbolic secant (HS) chirped pulses,[41,51] were used for the AL FRESCO experiments. While it was possible to obtain similar spectra using either one of these waveforms, it was generally seen that when directly mediated by ^{15}N-^{15}N interactions the HS performed slightly better, while when proceeding via ^{1}H-^{1}H mixing the WURST was better. Hence HS pulses were used in collecting the data shown in Figure 1, while WURST ones were used to collect the data in Figure 2. Both of these pulses were constructed using the Topspin's shaped pulse waveforming menu, with a dwell time (Δt) = $3/\nu_r$, sweep bandwidth (BW) = 40-80 kHz, and number of digital points (N) = $t_p/\Delta t$, where ν_r is the MAS spinning rate and t_p is the chirp pulse duration. Normally $t_p = \tau_{mix}$, where τ_{mix} is the mixing time; however, for long mixing times such as τ_{mix} = 5 s or 6.25 s, τ_{mix} was divided into *n* chirp pulses with an identical t_p and having a phase alternation scheme $X\bar{X}Y\bar{Y}$…, where X or Y is the initial phase of an individual chirp pulse and ζ (ζ= X or Y) and $\bar{\zeta}$ are a forwardly and backwardly swept chirped pulses, respectively. An HS pulse scheme with a 1~5 % of truncation level and a WURST pulse scheme with the smallest even amplitude power *n* = 2 were optimal for maximizing

^{15}N-^{15}N correlations when using these long mixing time. Since these WURST or HS schemes employed a weak rf pulse power (maximum amplitude ~ 5-20 kHz) regardless of the MAS rate, the effective rf pulse power ($\overline{\nu_{rf}^{env}}$) of the resultant chirped pulses was significantly low and allowed the total mixing period to be extended up to a few seconds without inducing any serious rf heating effect on the sample. For instance, the rf pulse strength of the HS pulse scheme used in Figure 1b was at its maximum amplitude 11 kHz; considering the amplitude shape of the HS pulse with a truncation level of 1 %, the effective rf pulse strength ($\overline{\nu_{rf}^{env}}$) employed for the overall mixing time was only 0.48 ×11 kHz = 5.3 kHz. More details in designing a suitable chirp pulse scheme for the AL FRESCO mixing scheme were described in a previous publication.[27] For the short chirp pulse scheme applied along the ^{15}N channel in the indirect $^{1}H^{N}$-$^{1}H^{N}$ mixing scheme, we employed $\Delta t = 1/\nu_r$, BW = 40-80 kHz, and $N = t_p/\Delta t$ with $\tau_{mix} = t_p$ ($\leq$ 2ms). In this case a WURST type with *n* = 80 was found optimal with $\nu_1(^{15}N)$ = 25 kHz based on our numerical simulations carried out on a model 6-spin cluster, $^{15}N_1{}^{1}H_1$-$^{15}N_2{}^{1}H_2$-$^{15}N_3{}^{1}H_3$, shown in the Supporting Figure S1.

Chemical shift assignments of GB1. To obtain backbone chemical shift assignments (N, C_α, C') for GB1, NCA and NCO experiments were used. Spectra were acquired and processed by TopSpin, and the processed frequency domain spectra were analyzed using the POKY suite (BUILD 082522) after conversion to the UCSF format.[52] The *BMRB entry download* button in the *Resonances* tab of POKY was used to import chemical shifts published by the Rienstra group (BMRB entry number 15380).[53] Then, we generated peaks with an assignment label by the *Transfer and Simulate* tool (two-letter-code *TA*) on NCA and NCO. During this peak propagation step, we performed re-referencing of the spectra (two-letter-code *st*), by comparing uniform chemical shift differences between signals on our spectra and the simulated peak positions. After

that, peak positions were fine-tuned by careful visual inspection. Figure S3 in the Supporting material illustrates assignments on representative NCA and NCO spectra.

Assignments of the ^{15}N-^{15}N and ^{15}N(^{1}H^{1}H)^{15}N spectra. To identify long-range signals on the ^{15}N-^{15}N and ^{15}N^{1}H^{1}H^{15}N spectra, GB1 coordinates were downloaded from the Protein Data Bank (PDB ID 2GI9) and hydrogen atoms attached using a POKY Notepad script *attach_hydrogen_to_pdb.py* available in the POKY github repository.[54] Then, the POKY Notepad script *ssnmr_NNpeak_maker_using_pdb.py,* which calculates interatomic distances and places peaks with an assignment label if two atoms are closer than the cutoff distance specified by the user, was applied, specifying 5 Å as a cutoff for the distance between two amide hydrogen atoms. Generated peaks were sorted by data heights in the peak list window of POKY, and only peaks falling on a signal were accepted.

Acknowledgement: This work was performed at the National High Magnetic Field Laboratory, which is supported by National Science Foundation Cooperative Agreement No. DMR-2128556 and the State of Florida. WL acknowledges a partial support from the National Science Foundation (Grant No. DBI-2051595). Supports from the Israel Science Foundation (grant 1874/22) and the Perlman Family Foundation are gratefully acknowledged by LF. LF holds the Bertha and Isadore Gudelsky Professorial Chair and heads the Clore Institute for High-Field Magnetic Resonance Imaging and Spectroscopy (Weizmann Institute) whose support is also acknowledged.

References

(1) Tycko, R.; Dabbagh, G. *Chem. Phys. Lett.* **1990**, *173*.

(2) Sun, B. Q.; Costa, P. R.; Kocisko, D.; Lansburt, P. T.; Griffin, R. G. *J. Chem. Phys.* **1995**, *102*.

(3) Kiihne, S. R.; Mehta, M. A.; Stringer, J. A.; Gregory, D. M.; Shiels, J. C.; Drobny, G. P. *J. Phys. Chem. A* **1998**, *102*.

(4) Bennett, A. E.; Ok, J. H.; Griffin, R. G.; Vega, S. *J. Chem. Phys.* **1992**, *96*, 8624.

(5) Nielsen, N. C.; Blldsøe, H.; Jakobsen, H. J.; Levitt, M. H. *J. Chem. Phys.* **1994**, *101*.

(6) Raleigh, D. P.; Levitt, M. H.; Griffin, R. *Chem. Phys. Lett.* **1988**, *146*, 71.

(7) Verel, R.; Baldus, M.; Ernst , M.; Meier, B. H. *Chem. Phys. Lett.* **1998**, *287*.

(8) Lee, Y. K.; Kurur, N. D.; Helmle, M.; Johannessen, O. G.; Nielsen, N. C.; Levitt, M. H. *Chem. Phys. Lett.* **1995**, *242*.

(9) Levitt, M. H. In *Encycl. Nucl. Magn. Reson.* 2002; Vol. 9, p 165.

(10) Szeverenyi, N. M.; Sullivan, M. J.; Maciel, G. E. *J. Magn. Reson.* **1982**, *47*, 462.

(11) Grommek, A.; Meier, B. H.; Ernst, M. *Chem. Phys. Lett.* **2006**, *427*, 404.

(12) Meier, B. H. *Polarization transfer and spin diffusion in solid state NMR*; Academic Press: New York, 1994; Vol. 18.

(13) Brinkmann, A.; Levitt, M. H. *J. Chem. Phys.* **2001**, *115*, 357.

(14) Tycko, R. *J. Phys. Chem. B* **2008**, *112*, 6114.

(15) Takegoshi, K.; Nakamura, S.; Terao, T. *Chem. Phys. Lett.* **2001**, *344*, 631.

(16) Takegoshi, K.; Nakamura, S.; Terao, T. *J. Chem. Phys.* **2003**, *118*, 2325.

(17) Morcombe, C. R.; Gaponenko, V.; Byrd, R. A.; Zilm, K. W. *J. Am. Chem. Soc.* **2004**, *126*, 7196.

(18) De Paëpe, G.; Lewandowski, J. R.; Loquet, A.; Böckman, A.; Griffin, R. G. *J. Chem. Phys.* **2008**, *129*, 245101.

(19) Lewandowski, J. R.; De Paëpe, G.; Eddy, M. T.; Struppe, J.; Maas, J. W.; Griffin, R. G. *J. Phys. Chem. B* **2009**, *113*, 9062.

(20) Weingarth, M.; Demco, D. E.; Bodenhausen, G.; Tekely, P. *Chem. Phys. Lett.* **2009**, *469*, 342.

(21) Weingarth, M.; Bodenhausen, G.; Tekely, P. *Chem. Phys. Lett.* **2010**, *488*, 10.

(22) Hu, B.; Lafon, O.; Trébosc, J.; Chen, Q.; Amoureux, J.-P. *J. Magn. Reson.* **2011**, *212*, 320.

(23) Hu, B.; Trébosc, J.; Lafon, O.; Chen, Q.; Masuda, Y.; Takegoshi, K.; Amoureux, J.-P. *ChemPhysChem* **2012**, *13*, 3585.

(24) Scholz, I.; Huber, M.; Manolikas, T.; Meier, B. H.; Ernst, M. *Chem. Phys. Lett.* **2008**, *460*, 278.

(25) Hou, G.; Sun, S.; Han, Y.; Byeon, I.-J.; Ahn, J.; Concel, J.; Samoson, A.; Gronenborn, A. M.; Polenova, T. *J. Am. Chem. Soc.* **2011**, *133*, 3943.

(26) Hou, G.; Yan, S.; Trébosc, J.; Amoureux, J.-P.; Polenova, T. *J. Magn. Reson.* **2013**, *232*, 18.

(27) Wi, S.; Frydman, L. *Chem. Phys. Chem.* **2020**, *21*, 284.

(28) Bayro, M. J.; Huber, M.; Ramachandran, R.; Davenport, T. C.; Meier, B. H.; Ernst, M.; Griffin, R. G. *J. Chem. Phys.* **2009**, *130*, 114506.
(29) Shen, M.; Liu, Q.; Trébosc, J.; Lafon, O.; Masuda, Y.; Takegoshi, K.; Amoureux, J.-P.; Hu, B.; Chen, Q. *Solid State Nucl. Magn. Reson.* **2013**, *55-56*, 42.
(30) Yan, X. J.; Hu, B. *Chinese J. Magn. Reson.* **2016**, *33*, 361.
(31) Reif, B.; Hohwy, M.; Jaroniec, C. P.; Rienstra, C. M.; Griffin, R. G. *J. Magn. Reson.* **2000**, *145*, 132.
(32) Franks, W. T.; Wylie, B. J.; Stellfox, S. A.; Rienstra, C. M. *J. Am. Chem. Soc.* **2006**, *128*, 3154.
(33) Lewandowski, J. R.; De Paëpe, G.; Eddy, M. T.; Griffin, R. G. *J. Am. Chem. Soc.* **2009**, *131*, 5769.
(34) Goldbourt, A.; Day, L. A.; McDermott, A. E. *J. Magn. Reson.* **2007**, *189*, 157.
(35) Giraud, N.; Blackledge, M.; Bockmann, A.; Emsey, L. *J. Magn. Reson.* **2007**, *184*, 51.
(36) Marulanda, D.; Tasayco, M. L.; McDermott, A.; Cataldi, M.; Arriaran, V.; Polenova, T. *J. Am. Chem. Soc.* **2004**, *126*, 16608.
(37) Siedel, K.; Etzkorn, M.; Heise, H.; Becker, S.; Baldus, M. *Chembiochem* **2005**, *6*, 1638.
(38) Donovan, K. J.; Silvers, R.; Linse, S.; Griffin, R. G. *J. Am. Chem. Soc.* **2017**, *139*, 6518.
(39) van Rossum, B.; Castellani, F.; Pauli, J.; Rehbein, K.; Hollander, J.; de Groot, H. J. M.; Oschkinat, H. *J. Biomol. NMR* **2003**, *25*, 217.
(40) Franks, W. T.; Zhou, D. H.; Wylie, B. J.; Money, B. G.; Graesser, D. T.; Frericks, H. L.; Sahota, G.; Rienstra, C. M. *J. Am. Chem. Soc.* **2005**, *127*, 12291.
(41) Kupce, E.; Freeman, R. *J. Magn. Reson. A* **1995**, *115*, 273.
(42) Baum, J.; Tycko, R.; Pines, A. *Phys. Rev. A* **1985**, *32*, 3435.
(43) Silver, M. S.; Joseph, R. I.; Hoult, D. I. *J. Magn. Reson.* **1984**, *59*, 347.
(44) de Boer, I.; Bosman, L.; Raap, J.; Oschkinat, H.; de Groot, H. J. M. *J. Magn. Reson.* **2002**, *157*, 286.
(45) Lange, A.; Seidel, K.; Verdier, L.; Luca, S.; Baldus, M. *J. Am. Chem. Soc.* **2003**, *125*, 12640.
(46) Aluas, M.; Tripon, C.; Griffin, J. M.; Filip, X.; Ladizhansky, V.; Griffin, R. G.; Brown, S. P.; Filip, C. *J. Magn. Reson.* **2009**, *199*, 173.
(47) Kobayashi, T.; Slowing, I. I.; Pruski, M. *J. Phys. Chem. C* **2017**, *121*, 24687.
(48) Fung, B. M.; Khitrin, A. K.; Ermolaev, K. *J. Magn. Reson.* **2000**, *142*, 97.
(49) Baldus, M.; Petkova, A. T.; Herzfeld, J.; Griffin, R. G. *Mol. Phys.* **1998**, *95*, 1197.
(50) Polenova, T. In *NMR Spectroscopy of Biological Solids*; Ramamoorthy, A., Ed.; CRC Talyor & Francis: Boca Ranton, London, New York, 2006, p 57.
(51) Garwood, M.; delaBarre, L. *J. Magn. Reson.* **2001**, *153*, 155.
(52) Lee, W.; Rahimi, M.; Lee, Y.; Chiu, A. *Bioinformatics* **2021**, *37*, 3041.
(53) Frericks-Schmidt, H. L.; Sperling, L. J.; Gao, Y. G.; Wylie, B. J.; Boettcher, J. M.; Wilson, S. R.; Rienstra, C. M. *J. Phys. Chem. B* **2007**, *111*, 14362.
(54) (https://github.com/pokynmr).

Supplementary Files

This is a list of supplementary files associated with this preprint. Click to download.

- SupportingInformationWiEtAl.pdf